Polymer 51 (2010) 655–664

Contents lists available at ScienceDirect

Polymer

journal homepage: www.elsevier.com/locate/polymer

Synthesis and processing of PMMA carbon nanotube nanocomposite foams

Changchun Zeng*, Nemat Hossieny, Chuck Zhang, Ben Wang

High Performance Materials Institute Florida State University, Department of Industrial and Manufacturing Engineering FAMU-FSU College of Engineering 2525 Pottsdamer St, Tallahassee, FL 32310, USA

ARTICLE INFO

Article history:
Received 8 November 2009
Received in revised form
21 December 2009
Accepted 22 December 2009
Available online 4 January 2010

Keywords:
Polymer nanocomposite foams
Microcellular foams
Carbon nanotubes

ABSTRACT

Poly(methyl methacrylate) (PMMA) multi-walled carbon nanotubes (MWCNTs) nanocomposites were synthesized by several methods using both pristine and surface functionalized carbon nanotubes (CNTs). Fourier transform infrared (FTIR) spectroscopy was used to characterize the presence and types of functional groups in functionalized MWCNTs, while the dispersion of MWCNTs in PMMA was characterized using scanning electron microscopy (SEM). The prepared nanocomposites were foamed using carbon dioxide (CO_2) as the foaming agent. The cell morphology was observed by SEM, and the cell size and cell density were calculated via image analysis. It was found that both the synthesis methods and CNTs surface functionalization affect the MWCNTs dispersion in the polymer matrix, which in turn profoundly influences the cell nucleation mechanism and cell morphology. The MWCNTs are efficient heterogeneous nucleation agents leading to increased cell density at low particle concentrations. A mixed mode of nucleation mechanism was observed in nanocomposite foams in which polymer rich and particle rich region co-exist due to insufficient particle dispersion. This leads to a bimodal cell size distribution. Uniform dispersion of MWCNTs can be achieved via synergistic combination of improving synthesis methodology and CNTs surface functionalization. Foams from these nanocomposites exhibit single modal cell size distribution and remarkably increased cell density and reduced cell size. An increase in cell density of ~70 times and reduction of cell size of ~80% was observed in nanocomposite foam with 1% MWCNTs.

Published by Elsevier Ltd.

1. Introduction

Polymer foams (or porous polymeric materials) are important materials in a variety of applications due to their inherent advantages, such as low density, high specific strength, light weight and materials savings, low thermal conductivity and good sound isolation. Foams are used in a wide range of applications including packaging, buoyancy, thermal insulation, acoustic attenuation, vibration damping, absorbents and membranes for separation [1]. Foams with nanometer sized voids are being studied for their potential applications as the next generation low dielectric constant materials [2]. However, a major drawback of polymeric foams compared to their bulk counterparts are that they suffer reduced mechanical properties and lower dimensional and thermal stability, which limit their range of applications.

Recently microcellular foams have attracted a great deal of attention. Microcellular foams, typically characterized by cell sizes smaller than 10 μm and cell densities larger than 10^9 cells/cm^3 [3], have provided improved mechanical properties, while significantly reducing the usage of material and minimizing the weight of the final foam product. Microcellular plastics have shown improved fatigue life and energy absorption [4,5], increased toughness [6,7] and high thermal stability [8]. A variety of polymers have been adopted for the production of microcellular foams, e.g., polystyrene (PS) [9–11], poly(methyl methacrylate) (PMMA) [12,13], poly(vinyl chloride) (PVC) [14], polycarbonate (PC) [15,16], poly(ethylene terephalate (PET) [8,17]. However, production of microcellular foams is quite challenging requiring stringent processing conditions, such as extremely high pressure drop rates with processing temperatures close to the glass transition temperatures [10,11]. This greatly limits the processing window and the attainable size of the foam products.

Polymer nanocomposite foams are a new class of materials has shown steady growth over the past several years. The incorporation of nanoparticles in polymeric foams offer several potential benefits and have been discussed in detail in a recent review paper [18]. Due to the nanoscale size, nanoparticles have been shown to be an excellent reinforcement for foam materials [19–21]. Additionally, due to their large aspect ratio, large surface area and high particle

* Corresponding author. Tel.: +1 (850)410 6273.
E-mail address: zeng@eng.fsu.edu (C. Zeng).

0032-3861/$ – see front matter Published by Elsevier Ltd.
doi:10.1016/j.polymer.2009.12.032

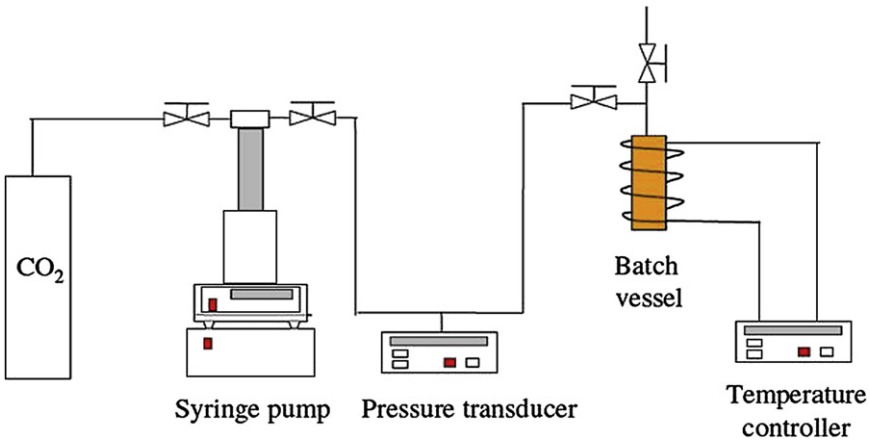

Fig. 1. Schematics of the high pressure foaming system.

concentration at low nominal particle concentration of the nanoparticles, they prove to be efficient agent for heterogeneous nucleation, leading to an increased cell density [22–24]. This nucleation efficiency is further increased by improved particle dispersion [23,25]. Via appropriate surface chemistry design of the nanoparticles, it is possible to achieve excellent dispersion and favorable polymer–nanoparticle–gas interactions that significantly reduces the nucleation free energy and increases nucleation rate [26]. Currently, most of the research in this area is focused on clay nanoparticles, though work on carbon nanofibers polymer nanocomposite foams have been reported [19,24,27,28].

Carbon nanotubes (CNTs) is another type of nanoparticle that has drawn tremendous interest in the research community because of their remarkable mechanical, electrical, magnetic, optical, and thermal properties [29]. Their exceptional properties, high aspect ratio (>1000), and the nanometer dimension make these materials ideal candidates for multifunctional reinforcements, as has been observed in a wide range of polymers [30]. It is envisaged that the incorporation of CNTs in polymers foams will lead to multifunctional materials with unrivaled properties that will greatly expand the use of polymeric foams. In addition, the different geometry and versatility of CNTs surface functionalization provide flexibility in tailoring the foam nucleation process to generate wide range of morphologies. Compared to the intensive investigation of polymer CNTs nanocomposites, the application of CNTs in polymer foam has only begun to emerge. Park et al. [31] prepared ethylene vinyl acetate (EVA) CNTs nanocomposite foams using pristine MWCNTs and observed significant increase in mechanical properties (tensile strength, tensile modulus, elastic recovery). CNTs nanocomposite foams based on poly (ε-caprolactone) (PCL) [32] and PS [33] were prepared using pristine MWCNTs and the nanocomposite foams show excellent electromagnetic shielding properties. Despite the promising initial reports, systematic study on the foam processing, structure and properties relationship in the presence of CNTs is largely unexplored.

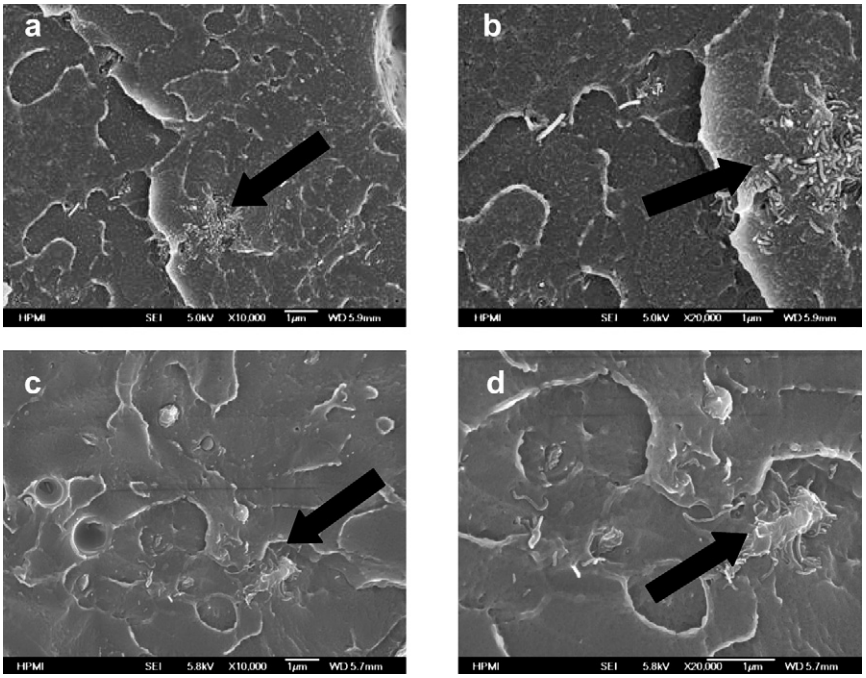

Fig. 2. Comparison of MWCNTs dispersion by solvent casting (a) and (b) and anti-solvent precipitation ((c) and (d)). Arrows indicate regions with MWCNTs aggregates. Magnification: (a), (c) 10,000x; (b), (d) 20,000x; Scale bars: 1 μm in all micrographs.

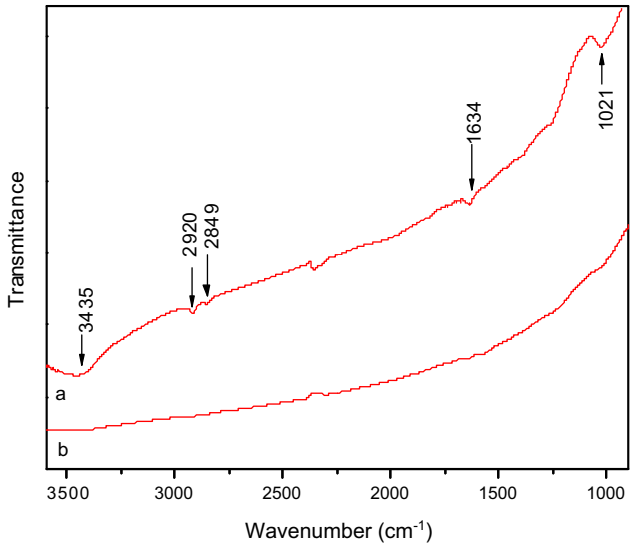

Fig. 3. FTIR spectra of (a) functionalized and (b) pristine MWCNTs.

In this study microcellular polymer CNTs nanocomposite foams based on poly (methyl methacrylate) (PMMA) and multi-walled carbon nanotubes (MWCNTs) were explored. Both pristine and surface functionalized CNTs were used in the nanocomposite fabrication. PMMA MWCNTs nanocomposites were first synthesized using several techniques, and nanocomposite foams were prepared by a batch foaming process. The foaming agent utilized was carbon dioxide, which attracted much attention as a physical blowing agent in polymer foaming [34] because of its low cost, abundance and environmentally benign nature [35]. The effects of foaming conditions and presence of different types of MWCNTs on the foam morphology were systematically investigated.

2. Experimental

2.1. Materials

The PMMA (Trade named Acrylite) used in the study were from Evonik Industries. Multi-walled carbon nanotubes (MWCNTs) with purity greater than 95% were purchased from Sigma–Aldrich. The nanotubes' inner and outer diameters were 5–10 nm and 10–30 nm, respectively. The length of the nanotubes ranged from 0.5 to 500 μm. Chloroform (HPLC Grade) was supplied by EMD Chemicals Inc. Bone dry grade carbon dioxide (i.e. 99% purity) was from Airgas Inc. Concentrated nitric and sulfuric acid were purchased from Fisher Scientific.

2.2. Synthesis of nanocomposites

Both pristine (pCNTs) and functionalized (fCNTs) MWCNTs were used for the nanocomposite synthesis. The fCNTs were prepared by an oxidization treatment of pCNTs with strong acids. In a typical procedure, 2 g of MWCNTs was suspended in a mixture of 150 ml of concentric HNO_3 and 50 ml of H_2SO_4 (3:1) and sonicated for 2 h. The MWCNTs were separated by filtration using a 0.2 μm PTFE membrane and washed with deionized water to remove all traces of acid. The resulting MWCNTs were then dried under a vacuum at 80 °C.

The nanocomposites were prepared using two methods: *solvent casting* (SC) and *anti-solvent precipitation* (ASP).

2.2.1. Solvent casting (SC)

PMMA was firstly dissolved in chloroform to form a homogeneous solution. MWCNTs were then added to the solution by magnetic stirring. The solution was further mixed with the added MWCNTs for 10 min followed by high power sonication (Misonix Sonicator 3000) for a period of 1 h. The polymer MWCNTs suspensions were casted in flat pans and kept in a fume hood to allow the solvent to evaporate. They were subsequently placed in a vacuum oven at 110 °C for 24 h for further solvent removal. The dried sample was then extruded using Mixing Extruder (LE-075, Custom Scientific Instruments) at 240 °C to remove any remaining solvent.

2.2.2. Anti-solvent precipitation (ASP)

The polymer MWCNTs suspension was prepared in a similar method to that described above. The suspension was then added drop-wise into a large volume of methanol (~10 mL of methanol was used for every 1 mL solution). The solution was continuously stirred vigorously using a mechanical stirrer. The methanol solution was further separated from the precipitated solids by filtration. The precipitates were dried in a vacuum and extruded to remove the solvent. The process is denoted as ASP.

A modified ASP process was conducted in a slightly different manner and was denoted as mASP. MWCNTs was suspended and sonicated in chloroform for extended period of time to form a stable suspension. PMMA solution was prepared in a separate container by dissolving PMMA in chloroform under magnetic stirring. The PMMA solution was then added to the MWCNTs suspension and underwent sonication for another 20 min. The mixture was then added drop-wise to a large amount of methanol. The remaining steps are similar to those for the original ASP.

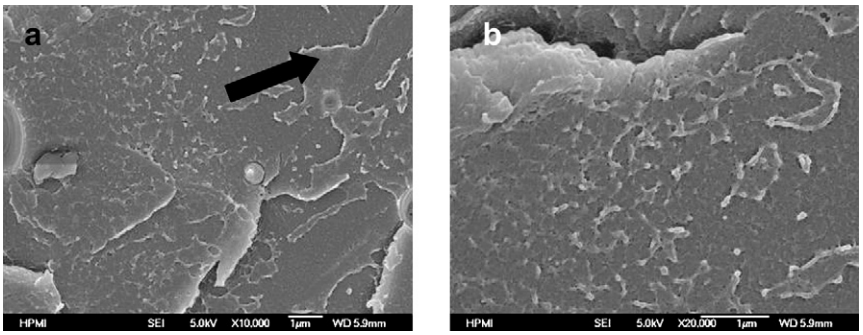

Fig. 4. Dispersion and distribution of fCNTs in PMMA by ASP; bright spots are fCNTs, while arrow indicates polymer rich region. Magnification (a)10,000x and (b) 20,000x; Scale bars: 1 μm in both micrographs.

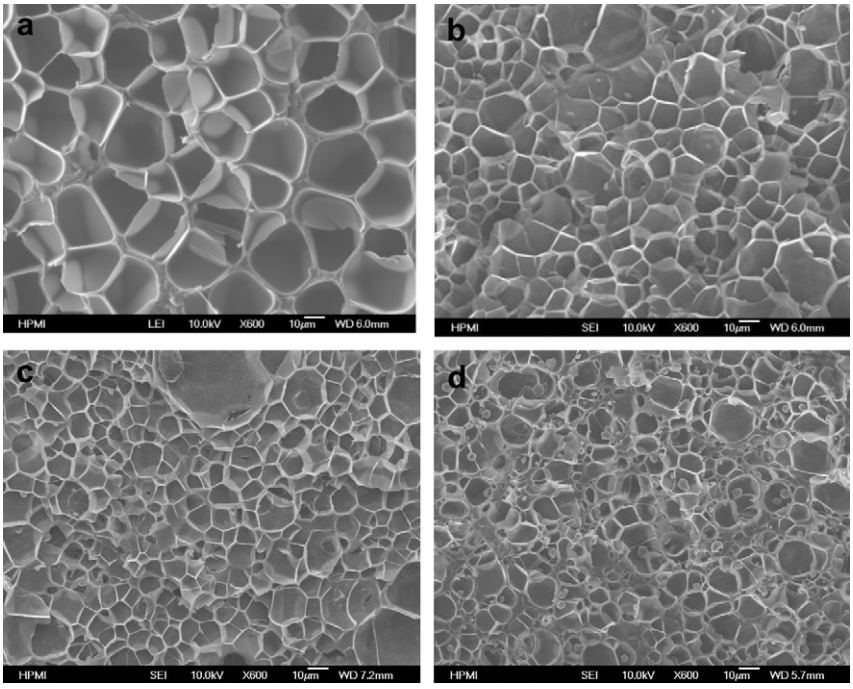

Fig. 5. Effect of pCNTs concentration on PMMA foams; (a) 0%; (b) 1%; (c) 2%; (d) 5%. Foams were prepared at 13.8 MPa and 120 °C; Scale bars: 10 μm in all micrographs.

2.3. Preparation of polymer MWCNTs nanocomposite foams

Batch foaming was conducted in a high pressure system as shown in Fig. 1. Samples were placed in the high pressure vessel. CO_2 was fed to the pressure vessel using an ISCO high pressure syringe pump and maintained at constant pressure. The system was kept at constant temperature (foaming temperature) for 20 h to allow CO_2 saturation and equilibrium. The pressure was then rapidly released and the foam morphology was fixed by cooling with an ice and water mixture.

2.4. Structural and morphological characterization

The morphology of the prepared polymer nanocomposite and nanocomposite foams was observed with a JOEL (JSM-7401 F) scanning electron microscope (SEM). The samples were fractured in liquid nitrogen and mounted on stubs and sputter coated with Au/Pd. Images were acquired at an accelerating voltage of 10 kV and a working distance of 8 mm.

Image analysis on the SEM micrograph was conducted to obtain the average cell size and cell density using Image J (National Institute of Health). Typically a micrograph showing more than 50 bubbles was chosen, and the number of bubbles, n, in the micrograph was determined by the software. If the area of the micrograph is A cm^2 and the magnification factor is M, the cell density can be estimated as

$$N_f = \left(\frac{nM^2}{A}\right)^{3/2} \quad (1)$$

FTIR spectra of the both pCNTs and fCNTs in KBr pellets were recorded by using a Nicolet 4700 FTIR spectrometer (Thermo Electron, Co., USA). The scan range was 400–4000 cm^{-1}.

3. Results and discussions

3.1. Preparation of nanocomposites

PMMA MWCNTs nanocomposites were prepared by both solvent casting and anti-solvent precipitation (ASP) using pristine MWCNTs (pCNTs) and were denoted as PMMA-sc-pCNT-x% and PMMA-asp-pCNT-x, respectively, in which sc stands for solvent

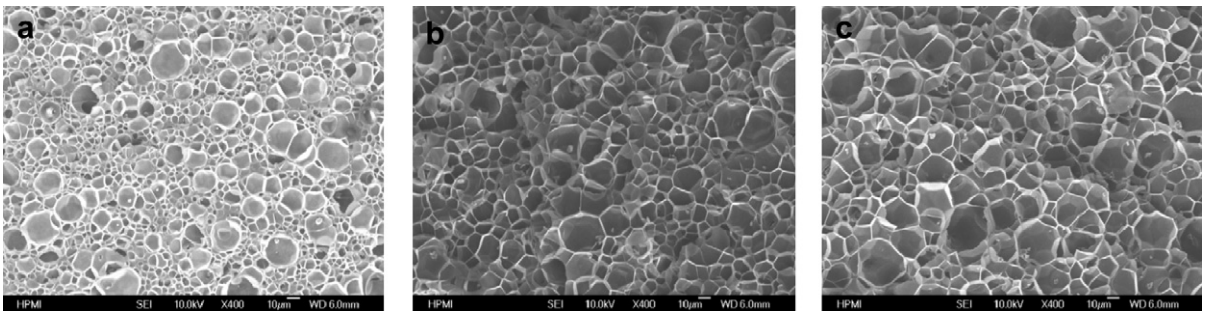

Fig. 6. Morphology of PMMA-asp-pCNT-1% nanocomposite foams prepared at 13.8 MPa and different temperatures, (a) 100 °C; (b) 120 °C; (c) 140 °C; Scale bars: 10 μm in all micrographs.

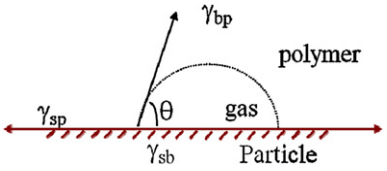

Fig. 7. Schematics of polymer–gas–particle interface; s: solid, b: bubble, p: polymer.

casting, asp stands for anti-solvent precipitation, p indicates pristine MWCNTs, and × denotes the weight concentration of CNT in the polymer. For example, PMMA-asp-pCNT-2% would be the PMMA MWCNTs nanocomposite prepared using anti-solvent precipitation and pristine MWCNTs with a weight concentration of 2%.

Due to their large surface area and strong van der Waals interaction, CNTs exist as bundles or agglomerates. An efficient dispersion method is of critical importance for achieving good dispersion of CNTs in polymers. High power sonication, one of the most commonly used methods for nanoparticles dispersion, is often employed in the nanocomposite preparation. However, in the solvent casting process, CNTs may re-aggregate as solvent evaporated due to thermodynamic reasons to reduce the surface free energy. This process may be slowed down or prevented by kinetic mechanism, provided the timescale to lock down (freeze) the structure is much smaller than that of re-aggregation. Thus, the anti-solvent precipitation process was employed. Instead of allowing solvent to evaporate, small drops of the suspension were added to an anti-solvent (methanol) in which the polymer is insoluble while the original solvent (chloroform) is soluble. It is envisaged that the rapid diffusion of chloroform into methanol leads to fast precipitation of small polymer/CNTs particles and slowing down of CNTs re-aggregation. The effect of processing methods on MWCNTs dispersion was investigated, and the results are shown in Fig. 2. MWCNTs aggregates were observed in each case. Apparently, neither process resulted in adequate MWCNTs dispersion in the polymer.

To improve CNTs dispersion, functionalization is routinely used to enhance the interaction between CNTs and polymers. In this study surface functionalization was conducted using mixed acid as described in the experimental section. The functionalized MWCNTs are denoted as fCNTs.

Fig. 3 shows the FTIR spectra of both pCNTs and fCNTs. Compared to the featureless spectrum of pCNTs, the fCNTs showed several peaks that are characteristics of several types of functional groups (hydroxyl, carboxyl and carbonyl) as previously reported [30]. The peak at 1634 cm^{-1} is assigned to the stretching vibration of the carbonyl group present in carboxylate ($-COO^-$). A broad peak at 3435 cm^{-1} corresponds to the stretching vibration of hydroxyl group (–OH). The peak at 1021 cm^{-1} is assigned to the stretch vibration of C–O group, which may have resulted from either the carboxyl or hydroxyl group attached to MWCNTs. It is well known that concentrated oxidizing acids such as the nitric acid and sulfuric acid used in the study are every effective in introducing acidic groups onto the surface of carbonaceous materials in general, and carbon nanotubes in particular, by successive oxidation [36]. And our results are in agreement with previous report [37] that the major functional groups from the acid treatment are carboxylic, phenolic and lactonic in nature. Functionalization of the MWCNTs is further supported by the presence of the small peak at 2920 cm^{-1}, which would result from stretching vibration of the methyl group, consistent with the breaking of sp^2 bond to form sp^3 bond by acid treatment. The increased polarity and the π-π interactions between the nanotubes and constitutive carbonyl unities of PMMA is expected to promote CNTs dispersion [38]. In addition, the favorable interaction between the carbonyl group and CO_2 by electron donor acceptor interaction [39] is beneficial for reducing contact angle and heterogeneous nucleation free energy [26].

The nanocomposites were prepared using fCNTs and ASP. Fig. 4 shows the SEM micrograph of the nanocomposites. While the MWCNTs are better dispersed (the bright spots in the micrograph), the distribution of MWCNTs is not uniform. Both MWCNTs rich and polymer rich (or MWCNTs deficient) regions are present.

3.2. Nanocomposite foams: bimodal morphology

Both pure polymer and nanocomposites were foamed using a batch process over a range of temperature and pressure conditions.

3.2.1. Effect of MWCNTs concentration

The PMMA nanocomposites with different MWCNTs concentrations (1%, 2%, 5%) were foamed at 120 °C and 13.8 MPa, and the respected cell morphology are shown in Fig. 5. While the pure PMMA foam exhibits a relatively uniform cell size, the nanocomposite foams show a bimodal cell size distribution in the presence of pCNTs: a large number of small cells are interspersed between a small number of big cells. Similar morphology has also been observed in EVA CNTs nanocomposite foams [31], while no significant change in cell size and cell density were reported by Wang et al. [40] for PMMA CNTs foams. The authors suggest that this is due to the fact that poor CNTs dispersion and large CNTs aggregates lead to negligible nucleation effect. As pCNTs concentration further increased to 5% (Fig. 5(d)), cell coalescence and interconnection became more prominent. This is similar to the results previously reported for clay nanocomposite foams [23], where the presence of a large number of anisotropic nanoparticles may facilitate directional cell growth, leading to enhanced cell impingements, wall rupture and cell coalescence.

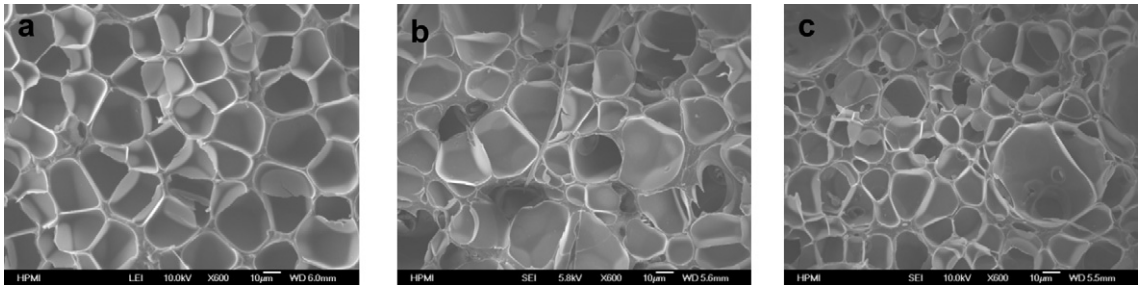

Fig. 8. Foam morphology of PMMA and nanocomposite foams prepared at 120 °C and 13.8 MPa; (a) pure PMMA; (b) PMMA-asp-pCNT-1%; (c) PMMA-asp-fCNT-1%; Scale bars: 10 μm in all micrographs.

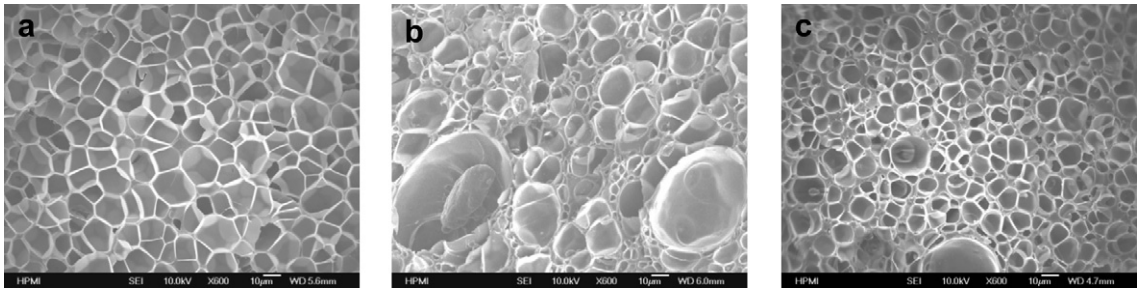

Fig. 9. Foam morphology of PMMA and nanocomposite foams prepared at 120 °C and 16.5 MPa; (a) pure PMMA; (b) PMMA-asp-pCNT-1%; (c) PMMA-asp-fCNT-1%; Scale bars: 10 μm in all micrographs.

To ascertain and confirm the observed bimodal distribution of cell size, the nanocomposite PMMA-asp-pCNT-1% was foamed under 13.8 MPa at a series of temperatures. Fig. 6 shows the cell morphologies. Bimodal cell size distribution is observed in each case.

The cell density or number of bubbles per unit volume is largely determined by the nucleation step in the foaming process. Nucleation is a classic phenomenon and exists in many processes, e.g., vapor condensation, crystallization. During nucleation, molecules overcome an energy barrier and group together (via local density and energy fluctuation) to form embryos of the new phase. When the sizes of the embryos are smaller than a critical size, an increase of embryo size is accompanied by an increase of free energy. On the other hand, if the size exceeds the critical size, further increase of embryo sizes lead to a reduction in free energy. Thus, stable nuclei are generated. Classical nucleation theory [41,42] was widely used in foaming to illustrate experimental phenomena due to its simplicity. According to the classical nucleation theory, the homogeneous nucleation rate is expressed as [43].

$$N_{\mathrm{hom}} = f_0 C_0 \exp\left(-\Delta G^*_{\mathrm{hom}}/kT\right) \tag{2}$$

Where f_0 is the frequency factor representing the frequency that gas molecules joining the embryo nucleus, C_0 is the concentration of the gas molecules, $\Delta G^*_{\mathrm{hom}}$ is the Gibbs free energy associated with the formation of a nucleus and is given by

$$\Delta G^*_{\mathrm{hom}} = \frac{16\pi}{3(\Delta P)^2}\gamma^3_{\mathrm{bp}} \tag{3}$$

Where γ_{bp} is the interfacial tension at the gas bubble polymer interface and ΔP is the pressure exerted by the gas on the cell walls.

In the presence of particles, bubbles may form at the polymer–particle interface (Fig. 7) following heterogeneous nucleation mechanism. The nucleation rate is expressed as [43,44]:

$$N_{\mathrm{het}} = f_1 C_1 \exp\left(-\Delta G^*_{\mathrm{het}}/kT\right) \tag{4}$$

Where f_1 has the similar physical meaning as f_0 in homogeneous nucleation; C_1 is the concentration of heterogeneous nucleation sites, which is directly related to the particle concentration. The Gibbs free energy for heterogeneous nucleation $\Delta G^*_{\mathrm{het}}$ is given by

$$\Delta G^*_{\mathrm{het}} = \frac{16\pi}{3(\Delta P)^2}\gamma^3_{\mathrm{bp}} f(\theta) \tag{5}$$

The presence of an interface thus greatly reduces the free energy for nucleation leading to an increase in nucleation rate.

The observed bimodal cell morphology may arise from a mixed mode nucleation mechanism in which simultaneous homogeneous and heterogeneous nucleation take place. In the PMMA MWCNTs nanocomposites, the MWCNTs are not well dispersed and form aggregates (Fig. 2). MWCNTs rich and MWCNTs deficient (polymer rich) regions co-exist. In the particle rich region, the more energetically favored heterogeneous nucleation dominates and the homogeneous nucleation is substantially suppressed as both processes compete for gas molecules to form nuclei. On the other hand, in the polymer rich regions, the initial fate of dissolved gas molecules is two-fold. Nuclei may form via homogeneous nucleation mechanism, or the dissolved gas may diffuse to the formed nuclei (from the heterogeneous nucleation mechanism) to support the growth. Despite the high nucleation free energy barrier, it is plausible that homogeneous nucleation could still takes place in polymer rich regime where particles are deficient, but at significantly lower rate, whilst the majority of the dissolved CO_2 may serves as reservoir to supply the growth of the limited number of nuclei formed through homogeneous nucleation rather than forming new nuclei. Hence, considerably fewer bubbles grow in the polymer rich region with ample supply of gas molecules, resulting in larger bubble size. On the other hand, in particle rich regions, simultaneous growth of a large number of

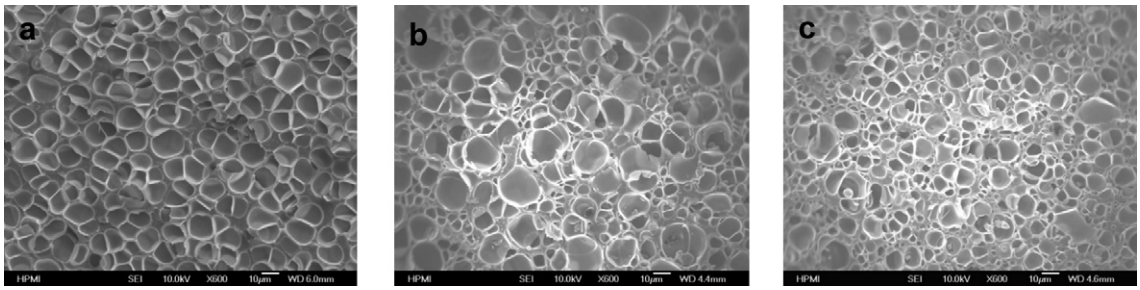

Fig. 10. Foam morphology of PMMA and nanocomposite foams prepared at 100 °C and 16.5 MPa; (a) pure PMMA; (b) PMMA-asp-pCNT-1%; (c) PMMA-asp-fCNT-1%; Scale bars: 10 μm in all micrographs.

Table 1
Cell size and cell density of PMMA MWCNTs nanocomposite foams.

Experiment condition ID[a]	Sample ID[b]	Distribution Type[c]	Cell size 1 (μm)[d]	Cell density 1 (cells/cm^3)	Cell size 2 (μm)[d]	Cell density 2 (cells/cm^3)
I	A	Mono	21.0 (6.4)	8.0×10^7	N/A	N/A
	B	Bi	16.8 (6.2)	1.4×10^8	33.0 (5.9)	8.0×10^6
	C	Bi	12.8 (5.1)	2.7×10^8	36.8 (8.9)	8.4×10^5
II	A	Mono	12.7 (3.2)	3.4×10^8	N/A	N/A
	B	Bi	7.6 (4.8)	7.6×10^8	18.6 (7.2)	3.4×10^7
	C	Bi	6.9 (2.4)	1.9×10^9	15.2 (5.5)	6.8×10^6
III	A	Mono	10.3 (2.1)	5.3×10^8	N/A	N/A
	B	Bi	5.7 (2.6)	2.3×10^9	17.1 (4.4)	1.5×10^7
	C	Bi	4.7 (2.6)	3.8×10^9	13.8 (3.9)	9.3×10^6

[a] Experimental conditions: I: 120 °C, 13.8 MPa, II: 120 °C, 16.5 MPa; III: 100 °C, 16.5 MPa.
[b] Sample ID: A: pure PMMA; B: PMMA-asp-pCNT-1%; C: PMMA-asp-fCNT-1%.
[c] Mono: mono-size distribution; bi: bimodal distribution.
[d] Standard deviation values in parenthesis.

bubbles leads to substantially smaller bubble size. It should be noted that mixed mode nucleation have been reported in the literature for polymer foams in the presence of micron sized particles [45]. These effects may be more prominent in foaming of nanocomposites because of the more technically challenging nature of achieving sufficient dispersion of nanoparticles.

Despite the bimodal cell size distribution resulting from insufficient MWCNTs dispersion, increased cell density in nanocomposite foams compared to that of the pure PMMA foam (Fig. 5) demonstrates the potential of the nucleation efficiency of MWCNTs, provided a strategy for better MWCNTs dispersion can be developed.

Table 2
Comparison of normalized cell size of PMMA and nanocomposite foams.

Experimental conditions ID / Sample ID	I	II	III
A	1	1	1
B	0.80	0.60	0.55
C	0.62	0.54	0.46

Table 3
Comparison of Normalized cell density of PMMA and nanocomposite foams.

Experimental conditions ID / Sample ID	I	II	III
A	1	1	1
B	1.7	2.2	4.3
C	3.4	5.6	7.2

3.2.2. *Effect of MWCNTs surface functionalization*

To improve the MWCNTs dispersion in PMMA, surface functionalization was conducted. The FTIR results (Fig. 3) clearly suggest the introduction of polar groups enhancing the polymer MWCNTs interaction. As discussed earlier, the enhanced interaction is beneficial for achieving a more uniform MWCNTs dispersion. Additionally, similar to the previous research on polystyrene nanoclay nanocomposite foams [26], a favorable interaction between CO_2 and the MWCNTs through the carbonyl group attached to the MWCNTs surface potentially leads to a reduction in heterogeneous nucleation free energy and significantly increases nucleation rate. Thus nanocomposites were prepared with the fCNTs using anti-solvent precipitation. A series of foams were prepared at various processing conditions and the results are shown in Figs. 8–10. Again, a bimodal cell size distribution was observed in each case.

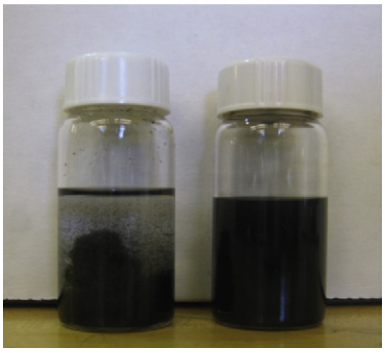

Fig. 12. Comparison of stability of nanocomposite suspension via ASP (left) and mASP (right). Material is PMMA-pCNT-1%.

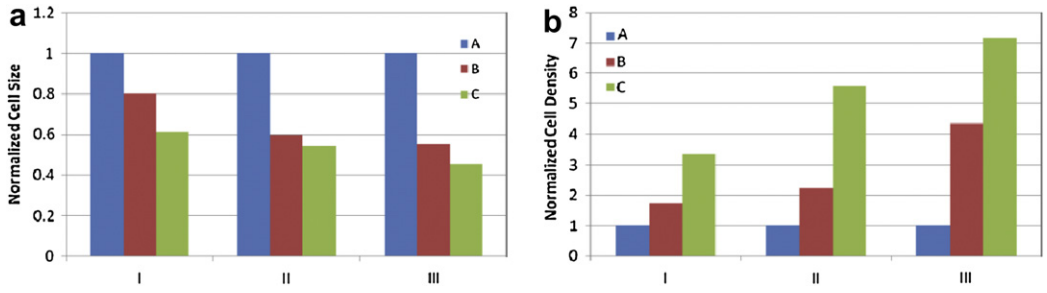

Fig. 11. Comparison of normalized cell size and cell density of PMMA and PMMA nanocomposite foams at a series of foaming conditions.

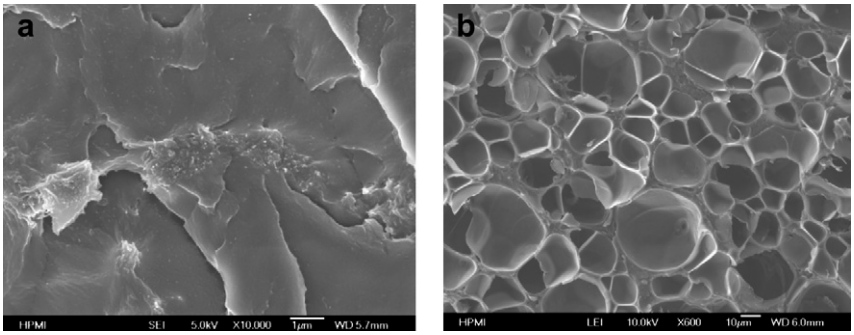

Fig. 13. SEM of PMMA-mASP-pCNT-1% nanocomposite (a) and nanocomposite foams (b) prepared at 120 °C and 13.8 MPa; Magnification: (a) 10,000x and (b) 800x; Scale bars: (a) 1 μm and (b) 10 μm.

Table 4
Effect of nanocomposites processing methods on the foam morphology.

Sample	Cell size distribution type	Cell size 1 (μm)[a]	Cell density 1 (#/cc^3)	Cell size 2 (μm)	Cell density 2 (#/cc^3)
Pure PMMA	Mono	21.0 (6.4)	8.0×10^7	N/A	N/A
PMMA-ASP-pCNT-1%	Bimodal	16.8 (6.2)	1.4×10^8	33.0 (5.9)	8.0×10^6
PMMA-mASP-pCNT-1%	Bimodal	11.6 (3.9)	1.7×10^8	24.7 (7.0)	1.7×10^7

[a] Standard deviation values in parenthesis.

To obtain more quantitative information on the cell morphology, image analysis was conducted to calculate the cell size and cell density of each mode and the results are summarized in Table 1. Furthermore, the size and density of model 1 cells were normalized using values of pure PMMA foam at respective foaming conditions as the reference, to further examine the role of MWCNTs. The results are shown in Tables 2 and 3 and Fig. 11.

Several observations were made on the role of MWCNTs on the reduction of cell size and the concurrent increase of cell density. First, the nucleation effect is more prominent when solubility of CO_2 in the polymer is higher. For example, at 120 °C and 13.8 MPa (condition I), samples B and C exhibit 0.7× and 2.4× increase of cell density compared to the pure PMMA foam. Increasing the saturation pressure from 13.8 MPa (I) to 16.5 MPa (II) lead to cell density increase of 1.2× and 4.6×, both values higher than those at condition I. Further increase of CO_2 solubility by lowering the temperature from 120 °C (II) to 100 °C (III) resulted in additional enhancement of nucleation efficiency (3.3× for sample B and 6.2× for sample C).

Furthermore, the PMMA-fCNTs nanocomposite foams (Sample C) consistently showed higher cell density and more reduction in cell size than PMMA-pCNTs foams (Sample B). This would be due to a combination of the following factors. First, the functionalized MWCNTs are better dispersed (albeit not uniformly) in PMMA, leading to an increase number of potential nucleation sites. Moreover, similar to the previous study on induction of carbonyl group onto nanoclay surface [26], the favorable interaction between CO_2 and the

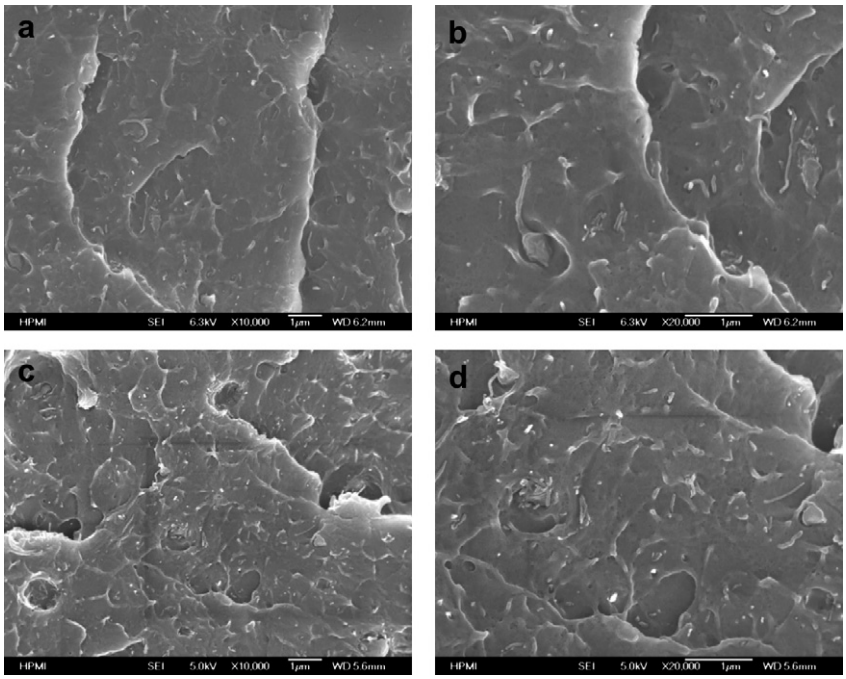

Fig. 14. SEM micrographs showing uniform MWCNTs dispersion via combination of surface functionalization and mASP; (a) and (b): PMMA-mASP-fCNT-1-2 h; (c) and (d): PMMA-mASP-fCNT-1-6 h; Scale bars: 1 μm in all micrographs.

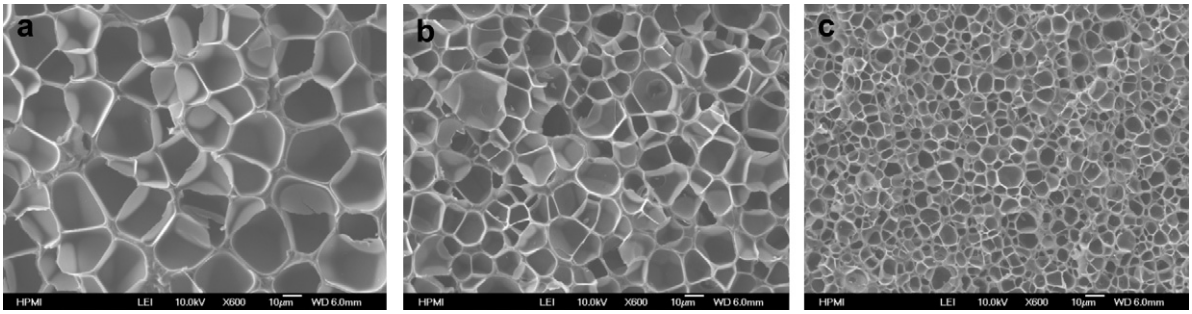

Fig. 15. Morphology of PMMA foams prepared at 120 °C and 13.8 MPa; (a) pure PMMA; (b) PMMA-mASP-fCNT-1%-2 h; (c) PMMA-mASP-fCNT-1%-6 h; Scale bars: 10 μm in all micrographs.

carbonyl group on MWCNTs may result in a reduction in the wetting angle and nucleation free energy and higher nucleation efficiency.

Regarding the other mode, the cell size of the nanocomposites foams were larger than that of the pure PMMA foam, while the cell densities were an order of magnitude lower. These are again in good agreement with the hypothesis that the large cells result from homogeneous nucleation mechanism, which has much lower rate due to the much higher nucleation free energy and therefore, being significantly suppressed in the presence of nanoparticles.

The fundamental reason for the mixed mode nucleation mechanism that leads to the bimodal cell size distribution is the presence of MWCNTs rich and MWCNTs deficient regime due to insufficient dispersion of MWCNTs. To effectively utilize the nucleation efficiency of the MWCNTs, a more effective strategy is required for more uniform MWCNTs dispersion.

3.3. Nanocomposite foams: mono-modal morphology

A modified ASP process (mASP) was employed to further improve MWCNTs dispersion. The major difference between mASP and the original ASP is that MWCNTs were first dispersed by sonication in solvent before the polymer solution was added. The MWCNTs were dispersed significantly better in the low viscosity solvent than in the polymer solution (the original ASP). Once dispersed and mixed with dissolved polymer, the polymer chains were able to wrap around the MWCNTs and stabilize the dispersion. Similar approaches have been adopted by other researchers [46] to prepare PMMA single walled carbon nanotubes (SWCNTs) nanocomposites and good dispersion was reported.

The uniformity of the MWCNTs dispersion was significantly improved via the modified process. Fig. 12 shows the comparison of the stability of PMMA-pCNT-1% suspension prepared by ASP and mASP. The former process resulted in precipitates exhibiting a grayish color indicating possible macroscopic phase separation, which completely settled down the bottom of the vial in a matter of minutes. On the other hand, the nanocomposite suspension from mASP shows a dark black color, and was extremely stable for an extended period of time. Shown in the figure is a sample that was still stable 12 weeks after preparation.

In spite of the great improvement of MWCNTs distribution, the MWCNTs rich region is still present. Fig. 13 shows SEM micrographs of the nanocomposites and the nanocomposite foams. MWCNTs aggregates were observed in the nanocomposites, and the nanocomposite foam exhibited a bimodal distribution of cell size.

The cell size and cell density of the foam were calculated via image analysis and compared to those of the nanocomposite foams by the original ASP. Table 4 shows the results. Albeit still possessing bimodal distribution, the nanocomposite from mASP process yielded foam with slight smaller of cell size and increase in cell density.

The dispersion of MWCNTs can be improved by either surface functionalization or refinement of nanocomposite synthesis methods; however, neither is adequate to produce nanocomposites with uniform MWCNTs dispersion. Further improvements in MWCNTs dispersion may result from combining the two aspects in nanocomposite preparation. Thus nanocomposites were synthesized using fCNTs via mASP processes. Two types of fCNTs were utilized: one treated with acid for 2 h and the other for 6 h. Both suspensions were very stable for extended periods of time. Fig. 14 shows the SEM micrographs of the two nanocomposites. Uniform dispersion of MWCNTs was observed for both nanocomposites. More nanotubes were observed in the nanocomposite in which MWCNTs underwent a 6 h acid treatment, suggesting possible breakage and shortening of MWCNTs.

Both nanocomposites were foamed at 13.8 MPa and 120 °C. The cell morphology is shown in Fig. 15 and compared with that of pure PMMA foam at the same processing conditions. Both foams show mono sized cell distribution with significantly higher cell density and smaller cell size.

Table 5 shows a quantitative analysis of the cell size and cell density. Compared to the pure PMMA foams, the cell size of the nanocomposite foam (PMMA-mASP-fCNT-1%-2 h) exhibit a reduction of cell size by ~44% and increase of cell density by 5.6 times. In spite of the observed nanotube breakage and shorting by prolonged surface functionalization by acid treatment for 6 h, the MWCNTs showed remarkable nucleation efficiency in the nanocomposite foam (PMMA-mASP-fCNT-1%-6 h). At 1% concentration, the cell size was reduced by ~80% (to ~4.5 μm) and cell density increased by ~70 times (to 5.4×10^9 cells/cm^3). Microcellular foams with uniform cell size distribution were successfully prepared under rather mild processing condition. Aside from the uniform particle dispersion, the following factors may further contribute to the exceptional nucleation efficiency observed: i) the breakage of MWCNTs leading to an increase in effective particle concentration and increase in number of nucleation sites; ii) extended functionalization leading to an increase of density of the functional groups,

Table 5
Comparison of characteristics of PMMA and PMMA MWCNTs nanocomposite foams.[a]

Sample	Cell size distribution type	Average cell size (μm)	Cell density (#/cc^3)
Pure PMMA	Mono	21.0	8.0×10^7
PMMA-mASP-fCNT-1%-2 h	Mono	11.6 (~44%)	4.5×10^8 (5.6x)
PMMA-mASP-fCNT-1%-6 h	Mono	4.5 (~78%)	5.4×10^9 (67.5×)

[a] Foams were prepared at 120 °C and 13.8 MPa. Nanocomposites were prepared by using fCNTs and mASP. Number in parenthesis show quantitatively the reduction of average cell size and increase of cell density.

which improve both particle dispersion and facilitate interaction with CO_2 to reduce heterogeneous nucleation free energy. The detail analysis of these effects will be presented in a separate paper.

4. Conclusions

In this study, PMMA MWCNTs nanocomposites were synthesized and novel PMMA MWCNTs nanocomposite foams were prepared in a batch foaming process using carbon dioxide as the foaming agent over wide range of foaming conditions. It was observed that the MWCNTs profoundly influenced the foam morphology. While MWCNTs are potentially efficient nucleation agents, the nucleation efficiency greatly depends on the dispersion of the MWCNTs in the polymer matrix. Bimodal cell size distribution was observed in the nanocomposite foams as a result of mixed mode of nucleation, which in turn resulted from the co-existence of MWCNTs rich and MWCNTs deficient (polymer rich) region due to insufficient MWCNTs dispersion. By appropriate MWCNTs surface functionalization and process improvement in nanocomposite synthesis, uniform MWCNTs dispersion in PMMA was achieved and outstanding nucleation efficiency of MWCNTs was observed in the nanocomposites foams ($\sim$80 times increase in cell density in the presence of 1% MWCNTs). Microcellular nanocomposite foams were prepared under mild processing conditions.

References

[1] Klempner D, Sendijarevic V. Handbook of polymeric foams and foam technology. Cincinnatti: Hanser Gardner Publications; 2004.
[2] Krause B, Koops G-H, van der Vegt NFA, Wessling M, Wubbenhorst M, van Turnhout J. Adv Mater 2002;14(15):1041–6.
[3] Martini-Vvedensky JE, Suh NP, Waldman FA. Microcellular closed cell foams and their method of manufacture. US; 1984.
[4] Seeler KA, Kumar VJ. J Reinf Plast Compos 1993;12(3):359–76.
[5] Matuana LM, Park CB, Balatinecz JJ. Cell Polym 1998;17(1):1–16.
[6] Baldwin DF, Suh NP. Annu Tech Conf – Soc Plast Eng 1992;50:1503–7.
[7] Collias DI, Baird DG. Polym Eng Sci 1995;35(14):1178–83.
[8] Shimbo M, Baldwin DF, Suh NP. Polym Eng Sci 1995;35(17):1387–93.
[9] Vipin K, Nam PS. Polym Eng Sci 1990;30(20):1323–9.
[10] Park CB, Baldwin DF, Suh NP. Polym Eng Sci 1995;35(5):432–40.
[11] Han X, Koelling KW, Tomasko DL, Lee LJ. Polym Eng Sci 2002;42(11):2094–106.
[12] Goel SK, Beckman EJ. Polym Eng Sci 1994;34(14):1137–47.
[13] Goel SK, Beckman EJ. Polym Eng Sci 1994;34(14):1148–56.
[14] Kumar V, Weller JE. Int Polym Process 1993;VIII(1):73–80.
[15] Kumar V, Weller J. J Eng for Ind 1994;116:413–20.
[16] Kumar V, VanderWel M, Weller J, Seeler KA. J Eng Mater Technol 1994;116(4):439–45.
[17] Kumar V, Schirmer HG. SPE-ANTEC, 53rd, vol. 2; 1995: pp. 2189–92.
[18] Lee LJ, Zeng C, Cao X, Han X, Shen J, Xu G. Compos Sci Technol 2005;65(15–16):2344–63.
[19] Shen J, Han X, Lee LJ. J Cell Plast 2006;42(2):105–26.
[20] Xu Z, Tang X, Gu A, Fang Z. J Appl Polym Sci 2007;106(1):439–47.
[21] Fu J, Naguib HE. J Cell Plast 2006;42(4):325–42.
[22] Zhai W, Yu J, Wu L, Ma W, He J. Polymer 2006;47(21):7580–9.
[23] Han X, Zeng C, Lee LJ, Koelling KW, Tomasko DL. Polym Eng Sci 2003;43(6):1261–75.
[24] Shen J, Zeng C, Lee LJ. Polymer 2005;46(14):5218–24.
[25] Lee SY, Xu YX, Hanna MA. Int Polym Process 2007;22(5):429–35.
[26] Zeng C, Han X, Lee LJ, Koelling KW, Tomasko DL. Adv Mater 2003;15(20):1743–7.
[27] Van Houten DJ, Baird DG. Polymer 2009;50(8):1868–76.
[28] Yang Y, Gupta MC, Dudley KL, Lawrence RW. Adv Mater 2005;17(16):1999–2003.
[29] Baughman RH, Zakhidov AA, de Heer WA. Science 2002;297(5582):787–92.
[30] Tasis D, Tagmatarchis N, Bianco A, Prato M. Chem Rev 2006;106(3):1105–36.
[31] Park K-W, Kim G- H. J Appl Polym Sci 2009;112(3):1845–9.
[32] Thomassin J-M, Pagnoulle C, Bednarz L, Huynen I, Jerome R, Detrembleur C. J Mater Chem 2008;18(7):792–6.
[33] Yang Y, Gupta MC, Dudley KL, Lawrence RW. Nano Lett 2005;5(11):2131–4.
[34] Tomasko DL, Han X, Liu D, Gao W. Curr Opin Solid State Mater Sci 2003;7(4–5):407–12.
[35] McHugh MA, Krukonis VJ. Supercritical fluid extraction: principle and practice. 2 ed. Stoneham, MA: Butterworths; 1994.
[36] Esumi K, Ishigami M, Nakajima A, Sawada K, Honda H. Carbon 1996;34(2):279–81.
[37] Shaffer MSP, Fan X, Windle AH. Carbon 1998;36(11):1603–12.
[38] Thomassin J-M, Lou X, Pagnoulle C, Saib A, Bednarz L, Huynen I, et al. J Phys Chem C 2007;111(30):11186–92.
[39] Kazarian SG, Brantley NH, West BL, Vincent MF, Eckert CA. Appl Spectrosc 1997;51:491.
[40] Wang X, Jana S, Sui G, Li W, Kumar V, Zhong WH. Proc Am Soc Compos. Tech Conf.; 2007, 22nd: 120/121–120/110.
[41] Abraham FF. Homogeneous nucleation theory. The pretransition theory of vapor condensation. Advances in theoretical chemistry, Suppl. 1. New York: Academic Press; 1974.
[42] Laaksonen A, Talanquer V, Oxtoby DW. Annu Rev Phys Chem 1995;46:489–524.
[43] Colton JS, Suh NP. Polym Eng Sci 1987;27(7):485–92.
[44] Colton JS, Suh NP. Polym Eng Sci 1987;27(7):493–9.
[45] Colton JS, Suh NP. Polym Eng Sci 1987;27(7):500–3.
[46] Kashiwagi T, Fagan J, Douglas JF, Yamamoto K, Heckert AN, Leigh SD, et al. Polymer 2007;48(16):4855–66.